Journal of Medicinal Chemistry Article

J. Med. Chem. **2011,** *54,* 331–341 **331**
DOI: 10.1021/jm101233f

Design, Synthesis, and Structural Analysis of Phenylpropanoic Acid-Type PPARγ-Selective Agonists: Discovery of Reversed Stereochemistry−Activity Relationship†

Masao Ohashi,‡ Takuji Oyama,§ Izumi Nakagome,∥ Mayumi Satoh,⊥ Yoshino Nishio,‡ Hiromi Nobusada,‡ Shuichi Hirono,∥ Kosuke Morikawa,§ Yuichi Hashimoto,# and Hiroyuki Miyachi*,‡

‡*Graduate School of Medicine, Dentistry and Pharmaceutical Sciences, Okayama University, 1-1-1, Tsushima-Naka, Kita-ku, Okayama 700-8530, Japan,* §*Institute for Protein Research, Osaka University, 6-2-3, Furuedai, Suita, Osaka 565-0874, Japan,* ∥*School of Pharmaceutical Sciences, Kitasato University, 5-9-1 Shirokane, Minato-ku, Tokyo 108-8641, Japan,* ⊥*Tumor Therapy Project, The Tokyo Metropolitan Institute of Medical Science, Tokyo Metropolitan Organization for Medical Research, 2-1-6 Kamikitazawa, Setagaya-ku, Tokyo 156-8506, Japan, and* #*Institute of Molecular and Cellular Biosciences, The University of Tokyo, 1-1-1, Yayoi, Bunkyo-ku, Tokyo 113-0032, Japan*

Received September 21, 2010

Peroxisome proliferator-activated receptor gamma (PPARγ) is a ligand-mediated transcription factor with roles in glucose, lipid, and lipoprotein homeostasis, and PPARγ ligands are expected have therapeutic potential in these as well as other areas. We report here the design, synthesis, crystallographic analysis, and computational studies of α-benzylphenylpropanoic acid PPARγ agonists. Interestingly, these compounds show a reversal of the stereochemistry−transactivation activity relationship observed with other phenylpropanoic acid ligands.

1. Introduction

The nuclear receptors (NRs[a]) form a superfamily of ligand-dependent transcription factors that control diverse biological functions, including reproduction, development, homeostasis, and immune function. This superfamily includes receptors for steroid hormones, thyroid hormones, retinoids, and vitamin D as well as a large number of orphan receptors. On the basis of the elucidated human genome sequence, 48 NRs are speculated to exist in humans.[1] Among them, much attention has been focused on the peroxisome proliferator-activated receptors (PPARs) over the past two decades, mainly because of their roles in glucose, lipid, and lipoprotein homeostasis.

PPARs are activated by endogenous saturated and unsaturated fatty acids and their metabolites as well as synthetic ligands.[2] Three subtypes, PPARα, PPARδ, and PPARγ, have been isolated to date, and each subtype appears to be differentially expressed in a tissue-specific manner. The most extensively studied subtype is PPARγ, which is expressed in adipose tissue, macrophages, vascular smooth muscle, and components of the immune system.[3] PPARγ is reported to be a principal regulator of adipocyte differentiation,[4] but recent molecular-biological studies have indicated that its activation is also linked to the expression of many important genes that affect energy metabolism, such as TNF-α, leptin, and adiponectin genes.[5]

The range of therapeutic potential for PPAR agonists is currently expanding well beyond lipid, lipoprotein, and glucose homeostasis, and PPAR biology and pharmacology are attracting enormous interest. For example, PPARγ activation attenuates the expression of inducible nitric oxide (iNOS) and cyclooxygenase-2 (COX-2) as well as the production of pro-inflammatory cytokines.[6] PPARγ was initially noted to be highly expressed in adipose tissue, but later studies demonstrated that PPARγ is also expressed widely in tumors originated from various organs. Ligand-mediated activation of PPARγ inhibits cell proliferation and/or induces apoptosis or terminal differentiation by upregulating the expression of cyclin-dependent kinase (CDK) inhibitors, including P18, P21, and P27.[7] PPARγ also promotes cell cycle arrest by inhibiting CDK activity in several tumor cell lines.[8] Angiogenesis, the formation of new blood vessels, is a critical step in solid tumor growth,[9] and PPARγ activation inhibits the expression of at least three important genes involved in angiogenic processes, i.e., VEGF, VEGF receptor 1, and urokinase plasminogen activator (uPA).[10] Therefore, PPARγ is considered as a therapeutic target for certain human malignancies. Further, on the basis of findings that the glitazone-class antidiabetic agents are ligands of PPARγ,[11] much research interest has been focused on NRs as therapeutic targets for the treatment of diabetes and dyslipidemia. These examples remind us that PPARs are pleiotropic NRs, and the PPAR subtypes appear to be potential, though somewhat overlapping, therapeutic targets for the treatment of not only metabolic disorders but also inflammation, cancer, neurodegeneration, wounds, etc. The range of possible applications of PPAR ligands has certainly not yet been fully explored.

We have been engaged in structural development studies of NR ligands (agonists and antagonists) for over 10 years, based

†PDB ID codes: 3AN3, hPPARγ LBD-(*S*)-**7**; 3AN4, hPPARγ LBD-(*R*)-**7**.

*To whom correspondence should be addressed. Phone: +81-086-251-7930. E-mail: miyachi@pharm.okayama-u.ac.jp

[a] Abbreviations: PPAR, peroxisome proliferator-activated receptor; NR, nuclear receptor; iNOS, inducible nitric oxide; COX-2, cyclooxygenase-2; CDK, cyclin-dependent kinase; VEGF, vascular endothelial growth factor; uPA, urokinase plasminogen activator; AF, activation function; DBD, DNA-binding domain; RE, response element; LBD, ligand-binding domain; THF, tetrahydrofurane; PDC, pyridinium dichromate; PDB, Protein Data Bank; JST, Japan Science and Technology Corporation; JSPS, Japan Society for the Promotion of Science.

Published on Web 12/03/2010

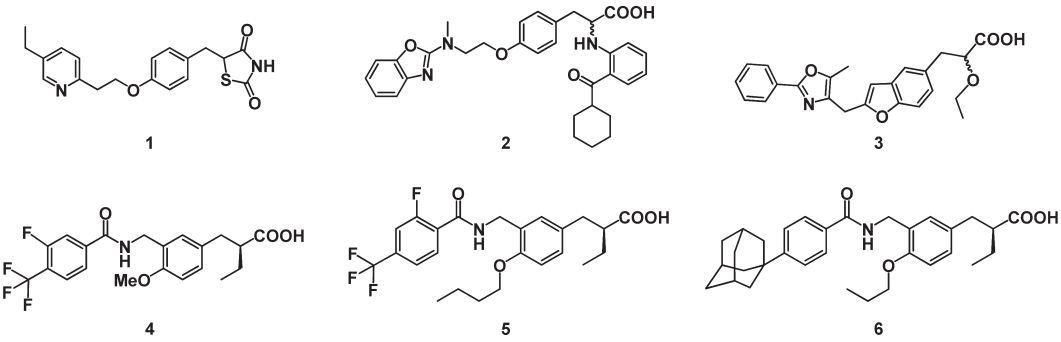

Figure 1. Representative PPARs agonists. **1**−**3**: PPARγ agonists. **4**: PPARα/δ dual agonist. **5**: PPARα/δ dual agonist. **6**: PPAR pan agonist.

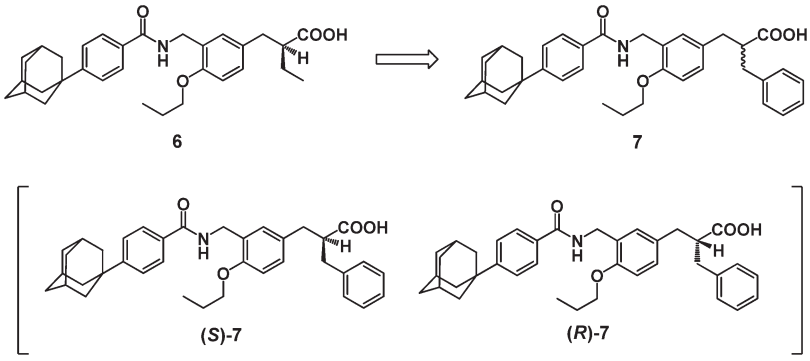

Figure 2. Our design concept for transition from PPAR pan agonist to PPARγ selective agonist.

on our working hypothesis concerning the NR ligand superfamily,[12] and we have already successfully designed and synthesized a series of substituted phenylpropanoic acid human PPARα-selective agonists,[13] PPARα/δ dual agonist,[14] PPARδ-selective agonists,[15] and PPAR $\alpha/\delta/\gamma$ pan agonist.[16] Here, we focus on phenylpropanoic acid-type PPAR agonists selective for the PPAR γ subtype.

In designing PPARγ-selective agonists, we started from our previously reported PPAR $\alpha/\delta/\gamma$ pan agonist **6** (Figure 1), which exhibited submicromolar EC_{50} values for all PPAR subtypes (EC_{50}s of the transactivation activity against hPPARα, hPPARδ, and hPPARγ are 61, 120, and 43 nM, respectively) (Figure 1). The appearance of the PPARγ activity of **6** was considered likely to have been due to the introduction of the sterically bulky adamantyl group at the hydrophobic tail part. Therefore we turned our attention to the substituent at the α-position of the carboxylic acid group. Considering the presence of the "benzophenone pocket" of the PPARγ-LBD,[17] we prepared several compounds with bulky substituents and found that the introduction of a benzyl group retained the PPARγ-agonistic activity while considerably decreasing the PPARα- and PPARδ-agonistic activities (data not shown) in the case of the racemic compound **7** (Figure 2).

In this paper, we present a series of optically active α-benzyl-substituted phenylpropanoic acid-type PPARγ-selective agonists. Interestingly, these compounds show a reversal of the stereochemistry−transactivation activity relationships previously reported for other phenylpropanoic acid ligands. This apparent discrepancy was resolved by means of X-ray crystallographic analysis and computational chemistry based on the obtained X-ray data.

2. Results and Discussion

2.1. Chemistry. Optically active α-benzylphenylpropanoic acid PPARγ-selective agonists, (*R*)-**7** and (*S*)-**7**, were prepared using Evans's asymmetric alkylation method[18] as the key step, as depicted in Scheme 1. 5-Formylsalicylic acid (**8**) was benzyl-esterified and *n*-propoxylated to give compound **9**. The formyl group of **9** was reduced with $NaBH_4$ (**10**) and bromination of the hydroxyl group afforded the bromomethyl derivative (**11**). (*S*)-*N*-3-Phenylpropionyl-4-benzyloxazolidinone was treated with **11** according to Evans's asymmetric alkylation protocol, followed by hydrogenolysis to afford benzoic acid derivative **13**. This was reduced with BH_3-THF (**14**), and then oxidation with PDC afforded the formyl derivative **14**. **14** was amide-alkylated with adamantan-1-ylbenzamide in the presence of trifluoroacetic acid and triethylsilane as the reducing agent, followed by removal of the chiral auxiliary to afford the desired (*R*)-configuration product (*R*)-**7** with 98% ee.[19] The antipodal (*S*) enantiomer was similarly prepared, using (*R*)-*N*-3-phenylpropionyl-4-benzyloxazolidinone as the reagent, with equivalent optical purity.

2.2. Biological Activities of (*R*)-7 and (*S*)-7. The PPARs transactivation activities of α-benzylphenylpropanoic acid (*R*)-**7** and (*S*)-**7**, together with the results for (*S*)-**6** (PPAR pan agonist) and rosiglitazone (PPARγ-selective agonist used clinically as an antidiabetic agent), are summarized in Figure 3.

Neither of the enantiomers exhibited apparent transactivation activity toward PPARα or PPARδ at the high concentration of 10 μM, while they both showed potent and selective PPARγ transactivation activity. The EC_{50} values of these compounds were similar or somewhat superior to those of the structurally similar PPAR pan agonist (*S*)-**6**. It is of particular interest that (*R*)-**7** is a more potent PPARγ-selective agonist than the antipodal (*S*)-enantiomer (the EC_{50} values of the transactivation activities of (*R*)-**7** and (*S*)-**7** for hPPARγ were 3.60 and 22.0 nM, respectively, in our assay system).

In agreement with the above result, (*R*)-**7** exhibited more potent 3T3-L1 adipocyte differentiation activity than (*S*)-**7**.

Scheme 1. Synthetic Route to the Present Series of Compounds[a]

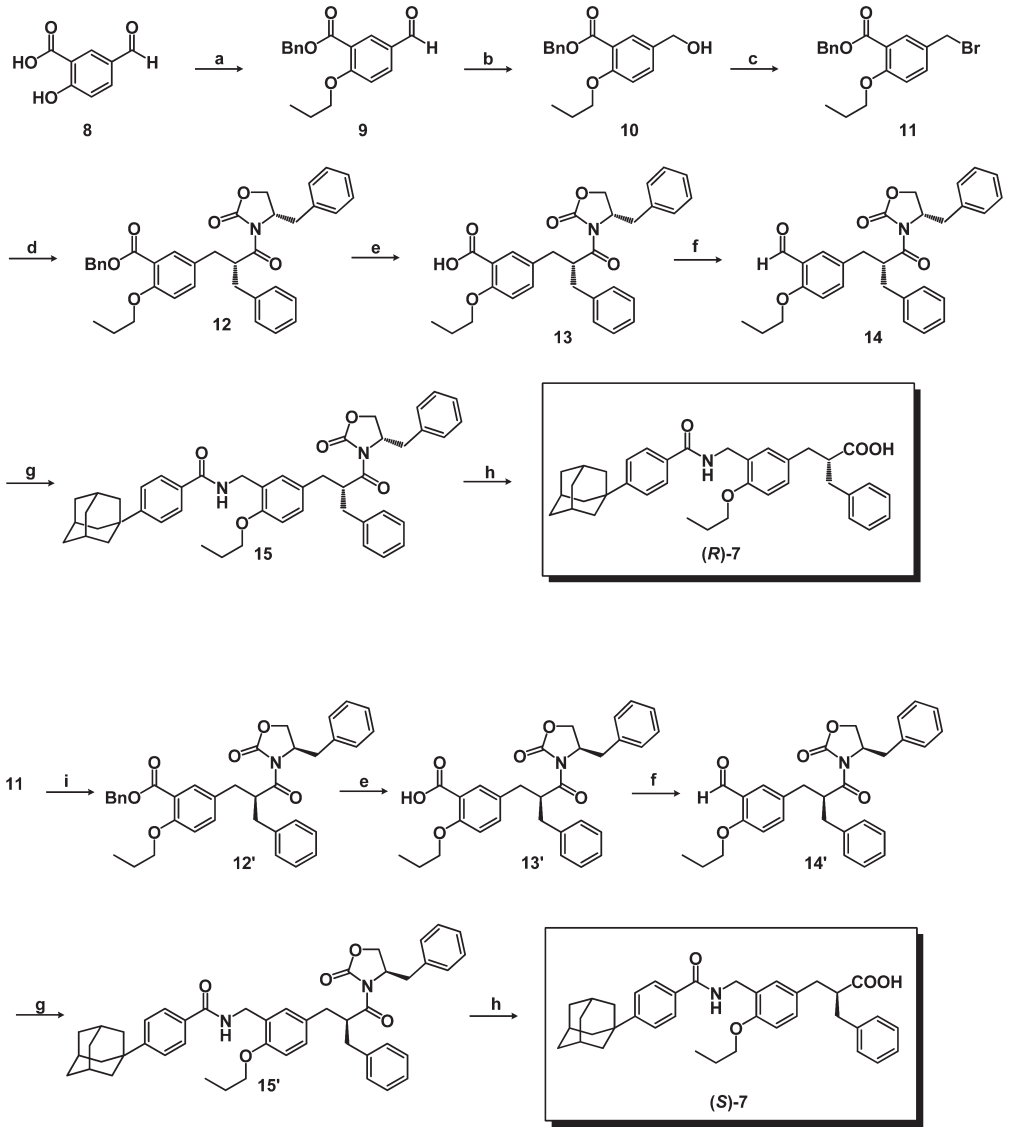

[a] Reagents and conditions: (a) (1) BnBr, $KHCO_3$, DMF, rt, overnight, quant, (2) *n*PrI, K_2CO_3, DMF, 60 °C, overnight, quant; (b) $NaBH_4$, EtOH, rt 2 h, 91%; (c) PBr_3, diethylether, 0 °C, 1.5 h, 52%; (d) (*R*)-3-(3-phenylpropanoyl)-4-benzyloxazolidin-2-one, LiHMDS, dehydrated THF, −50 °C to 0 °C, 2 h, 64%; (e) H_2, 10% Pd−C, AcOEt, rt, 3 h, 55%; (f) (1) BH_3-THF, dehydrated THF, 0 °C, overnight; (2) activated MnO_2,CH_2Cl_2, rt, overnight, 65% (2 steps); (g) 4-(1-adamantyl)benzamide, triethylsilane, TFA, toluene, reflux, 48 h, 97%; (h) LiOH-H_2O, 30% H_2O_2, THF:H_2O = 4:1 (v/v), 0 °C, 2.5 h then rt 3 h, 86%; (i) (*S*)-3-(3-phenylpropanoyl)-4-benzyloxazolidin-2-one, LiHMDS, dehydrated THF, −50 °C to 0 °C, 2 h, 70%.

As shown in Figure 4, (*R*)-7 exhibited maximum adipocyte differentiation activity at 100 nM, while a much higher concentration of (*S*)-**7** was needed for full activity.

Previous SAR data on our phenylpropanoic acid derivatives[13−16] indicated that the (*S*)-enantiomer is more potent than the (*R*)-enantiomer (see also Figure 3). For example, in the case of PPARα/δ dual agonist **4**, the (*S*)-enantiomer exhibited about 13-fold and 37-fold more potent PPARα and PPARδ transactivation activities, respectively, as compared with the (*R*)-enantiomer. In the case of PPARδ-selective agonist **5**, the (*S*)-enantiomer exhibited about 12-fold more potent activity than the (*R*)-enantiomer. As for the PPAR pan agonist **6**, the (*S*)-enantiomer is more potent than the (*R*)-enantiomer for all PPAR subtypes (about 8-fold, 7-fold, and 2-fold more potent for PPARα, PPARδ, and PPARγ transactivation activities, respectively). Although the activity of **6** resided primarily in the (*S*)-enantiomer, the enantioselectivity was less marked in the case of PPARγ.

These results are in good agreement with data reported for other series of PPARγ agonists. For example, in the case of tyrosine-based PPARγ agonists, exemplified by **2**, the (*S*)-enantiomer exhibited about 100-fold more potent binding activity, transactivation activity, and lipogenesis activity than the (*R*)-enantiomer.[21] In the case of the α-alkoxyphenylpropanoic acid-based PPARγ agonist series, exemplified by **3**, the (*S*)-enantiomer exhibited about 20-fold more potent glucose uptake activity as compared with the (*R*)-enantiomer.[22] Therefore, further studies were carried out to investigate the apparent reversal of the stereochemistry−activity relationship in the present compounds.

2.3. Binding of α-Alkylphenylpropanoic Acid Derivatives (*S*)-5 and (*S*)-6 to PPARs-LBD. To understand the (*S*)-conformational preference of our previous series, we had examined the three-dimensional structures of these phenylpropanoic acid PPAR ligands complexed with the corresponding PPAR subtype ligand-binding domains (LBDs) by means of

A

compd.	EC_{50} (nM) PPARα	PPARδ	PPARγ
(*S*)-7	ia	ia	22.0± 4.00
(*R*)-7	ia	ia	3.60± 1.10
(*S*)-6	54.0± 8.00	130± 40.0	41.0± 9.00
rosiglitazone	ia	ia	43.0± 3.00
(*S*)-4	12.0± 2.00	23.0± 8.00	ia
(*R*)-4	150± 10.0	840± 50.0	ia
(*S*)-5	250± 60.0	0.720± 0.08	ia
(*R*)-5	620± 60.0	8.50± 1.70	ia
(*S*)-6	54.0± 8.00	130± 40.0	41.0± 9.00
(*R*)-6	500± 50.0	870± 70.0	83.0± 10.0

B

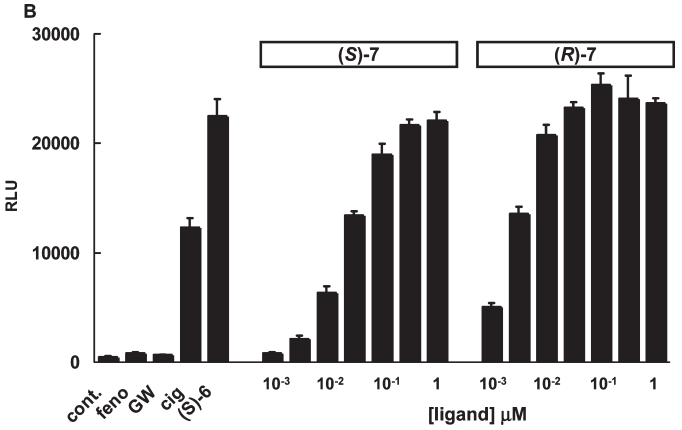

Figure 3. (A) Potency of (*S*)-**7**, (*R*)-**7**, and related compounds toward hPPARs. (B) Dose−response relationship of the hPPARγ transactivation activity. (A) Compounds were screened for agonist activity toward PPAR-GAL4 chimeric receptors in transiently transfected HEK-293 cells as described. The EC_{50} value is the molar concentration of the test compound that affords 50% of the maximal reporter activity. "ia" means inactive (no apparent activity) at the concentration of 10 μM. (B) abbreviations used are as follows: feno, 10^{-5} M fenofibrate (PPARα-selective agonist); GW, 10^{-7} M 2-(2-methyl-4-((4-methyl-2-(4-(trifluoromethyl)phenyl)thiazol-5-yl)methylthio)phenyl) acetic acid (GW-501516)[20] (PPARδ-selective agonist); Cig, 10^{-5} M ciglitazone (PPARγ-selective agonist); (*S*)-**6**, 10^{-6} M (*S*)-**6** (PPAR pan agonist).

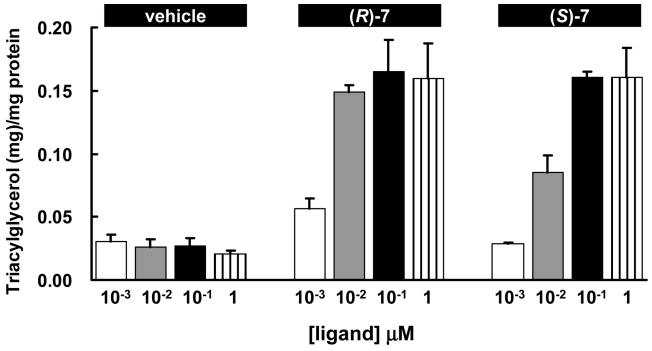

Figure 4. Dose-dependent induction of 3T3-L1 adipocyte differentiation by (*R*)-**7** and (*S*)-**7**. Data are expressed as mean ± SD ($n = 3$).

X-ray crystallographic analysis.[23] We succeeded in determining the three-dimensional structures of PPARα LBD−(*S*)-**6** complex, PPARδ LBD−(*S*)-**5** complex, and PPARγ LBD−(*S*)-**6** complex, as depicted in Figure 5A−G.[24] All three PPAR LBDs have similar folding of a three-layered sandwich comprising mainly α-helices, as also observed in the nuclear receptor LBDs (Figure 5A−D), and the overall interaction modes of the proteins with the ligands are substantially conserved.

The ligand-binding domains form Y-shaped pockets. The longest arm is placed behind helix 3, where the bound PPAR ligands specifically contact both hydrophilic and hydrophobic residues.[25] In particular, the hydrogen-bonding network contains the Tyr residue on the AF-2 helix (helix 12), which plays a key role in interacting with the carboxyl group of the ligand. The second arm, which is hydrophilic, is located on the opposite side to the first arm, against helix 3. The hydrophobic third arm lies at the entrance (H2′ and β-turns) to the binding pocket.

All three phenylpropanoic acid-type PPAR agonists show very similar ligand-binding modes. The acidic head carboxyl groups are located in the first cavity, making conventional interactions with the polar side chains, and thus all three PPAR LBDs adopt the conventional fully active conformation of helix 12 (Figure 5A−C). The central benzene rings and the alkoxy groups are located in the center and the second cavity, respectively, and the hydrophobic tail part lies at the entrance of the LBDs.

Parts E−G of Figure 5 present close-up views of compounds (*S*)-**5** and (*S*)-**6** complexed with PPARα-, PPARδ-, and PPARγ-LBD, respectively. Notably, these studies are consistent with the enantioselectivity of the compounds. The ethyl group in the (*S*)-enantiomer is located at the longest binding site with the head carboxyl group, forming hydrophobic interactions with the surrounding hydrophobic residues. When the (*R*)-enantiomer approaches the ligand-binding pocket, the terminal methyl group of the α-position ethyl group may interfere sterically with the surrounding residues, particularly with the side chains of the Cys residues in the central part of the H3 helix (Cys276, Cys285, and Cys285 of PPARα-, PPARδ-, and PPARγ-LBD, respectively).

2.4. Binding of (*S*)-7 and (*R*)-7 to PPARγ-LBD. The insight obtained from the studies on the α-ethylphenyl propanoic acid series **5** and **6** could not explain the discrepancy arising from the incorporation of a benzyl substituent at the α-position of the phenylpropanoic acid. Therefore, we conducted an X-ray crystallographic analysis of (*R*)-**7** and (*S*)-**7** complexed with the PPARγ LBD. PPARγ LBD-(*R*)-**7** and PPARγ LBD-(*S*)-**7** complexes were cocrystallized under the same conditions, as described in the Experimental Section. The crystallographic data and refinement statistics are summarized in Table 1.

2.5. Structural Basis for the Full-Agonistic Activity of α-Benzylphenylpropanoic Acid. Transcriptional activation at a nuclear receptor is a complex process, elicited initially by the binding of a ligand. After ligand binding, conformational change of the nuclear receptor occurs, which facilitates dissociation of the corepressor complex and subsequent recruitment of the coactivator complex.[26] The qualitative nature of the corepressor dissociation and coactivator recruitment was reported to be regulated differentially by the three-dimensional structure around the C-terminal H12 helix and the surrounding helixes of the nuclear receptor.[27] In the case of the binding of a full agonist, such as rosiglitazone, the H12 helix is stabilized by tight hydrogen bonding to Tyr473, and the H12 helix is docked properly against the H3 helix and H11 helix.[26] In this conformation, H12 forms part of the coactivator-binding surface along with the H3 helix and H5 helix. The positions of two distinct amino acids, Lys301 (in H3 helix) and Glu471 (in H12 helix), are especially important because

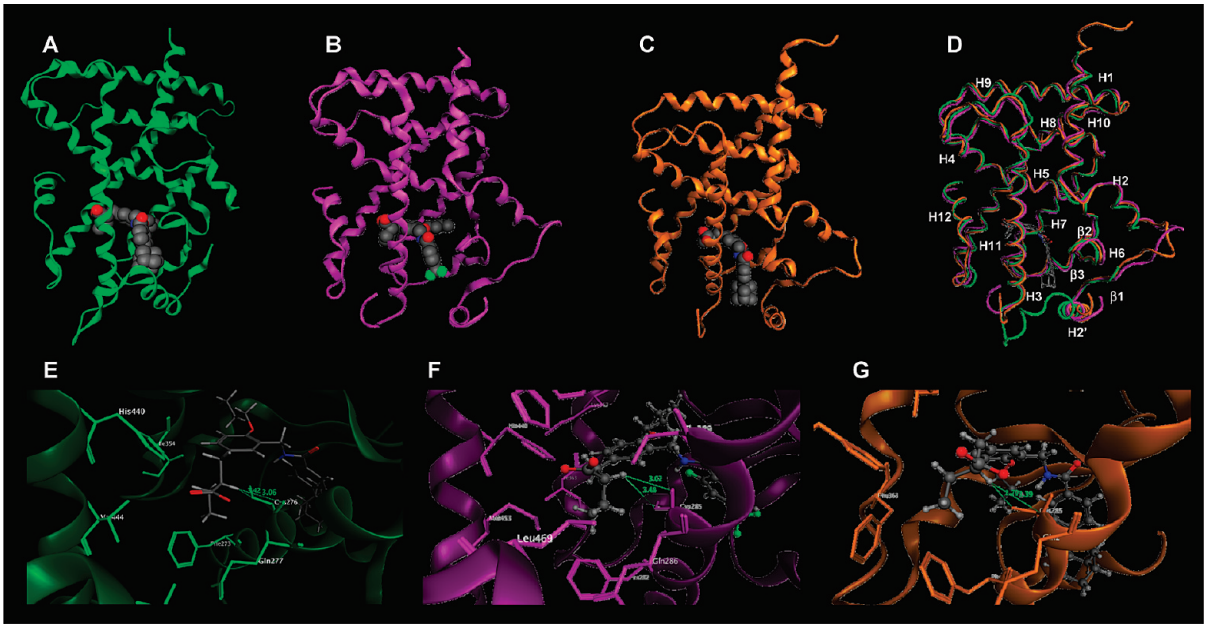

Figure 5. (A−C) Crystal structures of PPARs LBD−TIPP complexes. (A) PPARα LBD−(*S*)-**6** complex; (B) PPARδ LBD−(*S*)-**5** complex; (C) PPARγ LBD−(*S*)-**6** complex. Proteins are represented as ribbon models and the ligands are depicted as space-filling models, with F, C, N, and O atoms in aqua, gray, blue, and red, respectively. (D) Superposition of the main chains of each PPARs LBD. The numbering of the second structure is also depicted. (E−G) Zoomed view of the ligand-binding mode of PPARs LBD−TIPP complexes. (E) PPARα LBD−(*S*)-**6** complex; (F) PPARδ LBD−(*S*)-**5** complex; (G) PPARγ LBD−(*S*)-**6** complex. Proteins are represented as ribbon models and the ligands are depicted as cylinder models, with F, C, N, and O atoms in aqua, gray, blue, and red, respectively.

Table 1. Crystallographic Data and Refinement Statistics (Values in Parentheses Are for the Last Shell)

	PPARγ LBD-(*S*)-**7**	PPARγ LBD-(*R*)-**7**
	Data Collection	
space group	*C*2	*C*2
unit cell constants (Å)		
a	93.192	93.391
b	61.061	61.271
c	118.618	118.871
β (deg)	102.82	102.82102
wavelength (Å)	1	1
resolution (Å)[a]	50.0−2.30 (2.38−2.30)	50.0−2.30 (2.38−2.30)
no. of unique reflections	28907(2841)	28731(2825)
completeness (%)	99.3 (98.7)	97.8 (97.5)
$I/\sigma(I)$	32.7(6.6)	23.6(7.0)
redundancy	3.7 (3.3)	3.7 (3.4)
R_{merge} (%)[b]	3.0 (24.0)	3.5 (23.1)
	Refinement	
resolution range (Å)	50.0−2.30	50.0−2.30
R_{work}[c]/R_{free}[d]	22.7/27.8	23.2/28.8
no. of atoms		
protein	4155	4150
water	132	83
ligand	42	42
average *B*-factor (Å)		
protein	47.54	45.19
water	45.26	40.31
ligand	69.78	62.55
rmsd		
bond lengths (Å)	0.007	0.007
angles (deg)	1.1	1.1
PDB code	3AN3	3AN4

[a] Values in parentheses correspond to the last shell. [b] $R_{merge} = (\sum|I_I - \langle I_I\rangle|)/\sum_I |I_I|$ where $\langle I_I\rangle$ is the mean I_I over symmetry-equivalent reflections. [c] $R_{work} = \sum||F_o| - |F_c||/\sum|F_o|$ for all data excluding data to used to calculate R_{free}. [d] $R_{free} = \sum||F_o| - |F_c||/\sum|F_o|$ for all data

these amino acids clamp the LXXLL motif involved in the coactivators.

The framework of hPPARγ LBD complexed with (*S*)-**7** or (*R*)-**7** is depicted in Figure 6B,C, together with the structure of rosiglitazone−hPPARγ LBD complex (PDB: 2PRG, Figure 6A). Figure 6D shows a superposition of these three complexes (side chains of amino acids except those of Lys301 and Glu471 are omitted). The overall foldings of hPPARγ LBD complexed with (*S*)-**7** or (*R*)-**7** and rosiglitazone are well matched, except for the thermodynamically unstable region from the end of the H2 helix to the beginning of the H3 helix. The positions of the important amino acids for coactivator binding, Lys301 in the H3 helix and Glu471 in the H12 helix, overlap well in these structures. These structural-biological findings support the functional studies depicted in Figure 3B, indicating that both (*S*)-**7** and (*R*)-**7** function as full agonists.

2.6. Structural Basis for the PPARγ Selectivity and Potency of α-Benzylphenylpropanoic Acid. As mentioned above, α-ethylphenylpropanoic acid derivative **6** exhibited transactivation activities toward all PPAR subtypes, while α-benzylphenylpropanoic acid derivative **7** specifically transactivated PPARγ, being a more potent activator of PPARγ than was **6**. It appears that these differences in selectivity and activity can be mainly attributed to the difference of the interaction potential of the side chain at the α-position of phenylpropanoic acid with the surrounding amino acids. Parts B and C of Figure 6 show superposition of the amino acids of hPPARγ interacting with the benzyl group of (*S*)-**7** (α-substituent binding pocket) and the corresponding amino acids of hPPARδ and hPPARα (Figure 6B; hPPARδ vs hPPARα, Figure 6C; hPPARγ vs hPPARα). The volume of the α-substituent-binding pocket of hPPARδ is smaller than that of hPPARα due to the bulky Met residue (Val in hPPARα) located at the bottom of the pocket. The bulky benzyl side

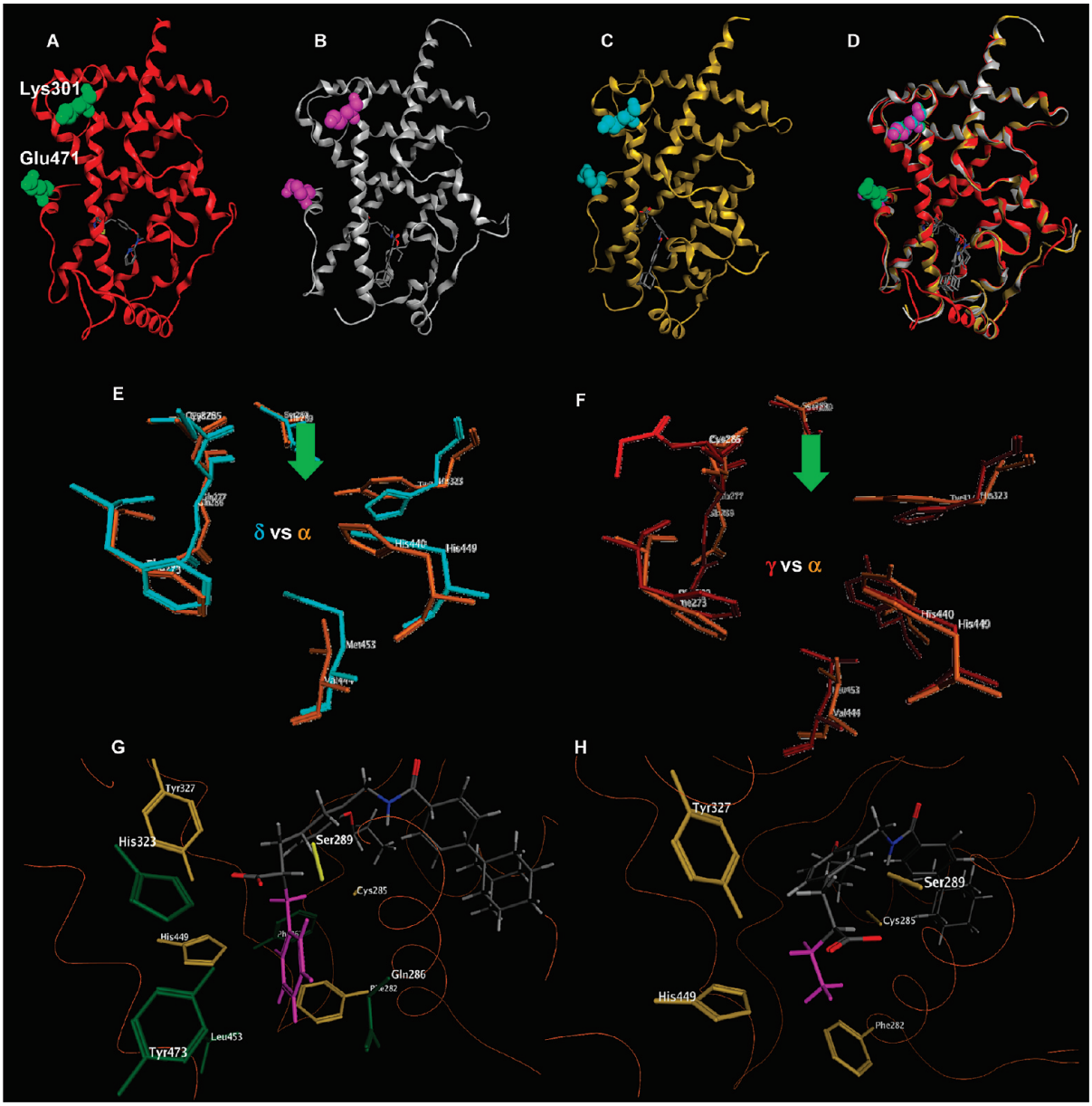

Figure 6. (A−C) Overall crystal structures of PPARγ LBD−ligand complexes. (A) PPARγ LBD−rosiglitazone complex (PDB 2PRG); (B) PPARγ LBD−(*S*)-**7** complex; (C) PPARγ LBD−(*R*)-**7** complex. Main chains of the proteins are represented, and each of the two amino acids Lys301 and Glu473 are highlighted as space-filling models, with green (rosiglitazone complex), magenta ((*S*)-**7** complex), and cyan ((*R*)-**7** complex). (D) Superposition of the main chains of each PPARγ LBD. (E−F) Zoomed views of the superposed amino acid residues forming the benzyl group-binding pockets. (E) Superposition of the PPARδ LBD (cyan) and PPARα LBD (orange). (F) Superposition of the PPARγ LBD (red) and PPARα LBD (orange). Protein backbones are omitted, and the side-chain amino acids are represented as cylinder models. (G−H) Zoomed views of the amino acids involved in the interaction of the side chain of the ligands. (E) Zoomed view of PPARγ LBD−(*S*)-**7** complex. (F) Zoomed view of PPARγ LBD−(*S*)-**6** complex. Proteins are represented as wireframe models and the amino acids interacting with the side-chain ethyl group of (S)-**6** are depicted as yellow cylinders, and the additional amino acid side chains interacted are depicted as green cylinders.

chain of (*S*)-**7** might not fit into the pocket of hPPARδ owing to steric interference with the side chain of the Met residue. It could also be considered that the width of the entrance of hPPARα is smaller than that of hPPARδ due to the bulky Tyr residue (His in hPPARδ) located at the entrance of the pocket. The bulky benzyl side chain of (*S*)-**7** might not be able to enter the pocket of hPPARα due to steric interference with the side chain of the Tyr residue.

These results clearly explain why the activity toward hPPARγ is improved by replacing the side chain at the α-position of the phenylpropanoic acids. In the case of (*S*)-**6**, the ethyl group interacts with the hydrophobic cavity composed of Phe282, Cys285, Ser289, Tyr327, and His449 (Tyr327 and His449 also contribute to the hydrogen-bonding network of the acidic carboxyl group of (*S*)-**6**) (Figure 6E). On the other hand, in the case of (*S*)-**7**, the benzyl group is wider than the ethyl group, and therefore the benzyl group interacts further with the additional hydrophobic cavity composed of Gln286, His323, Phe363, Leu453, and Tyr473. This expansion of the interaction area might be the main reason for the increase in the activity of (*S*)-**7** versus (*S*)-**6** (Figure 6D).

2.7. Comparison of the Structures of hPPARγ LBD Complexed with (*S*)-7 and (*R*)-7. The overall structures of hPPARγ LBD complexed with (*S*)-**7** and (*R*)-**7** are shown in parts

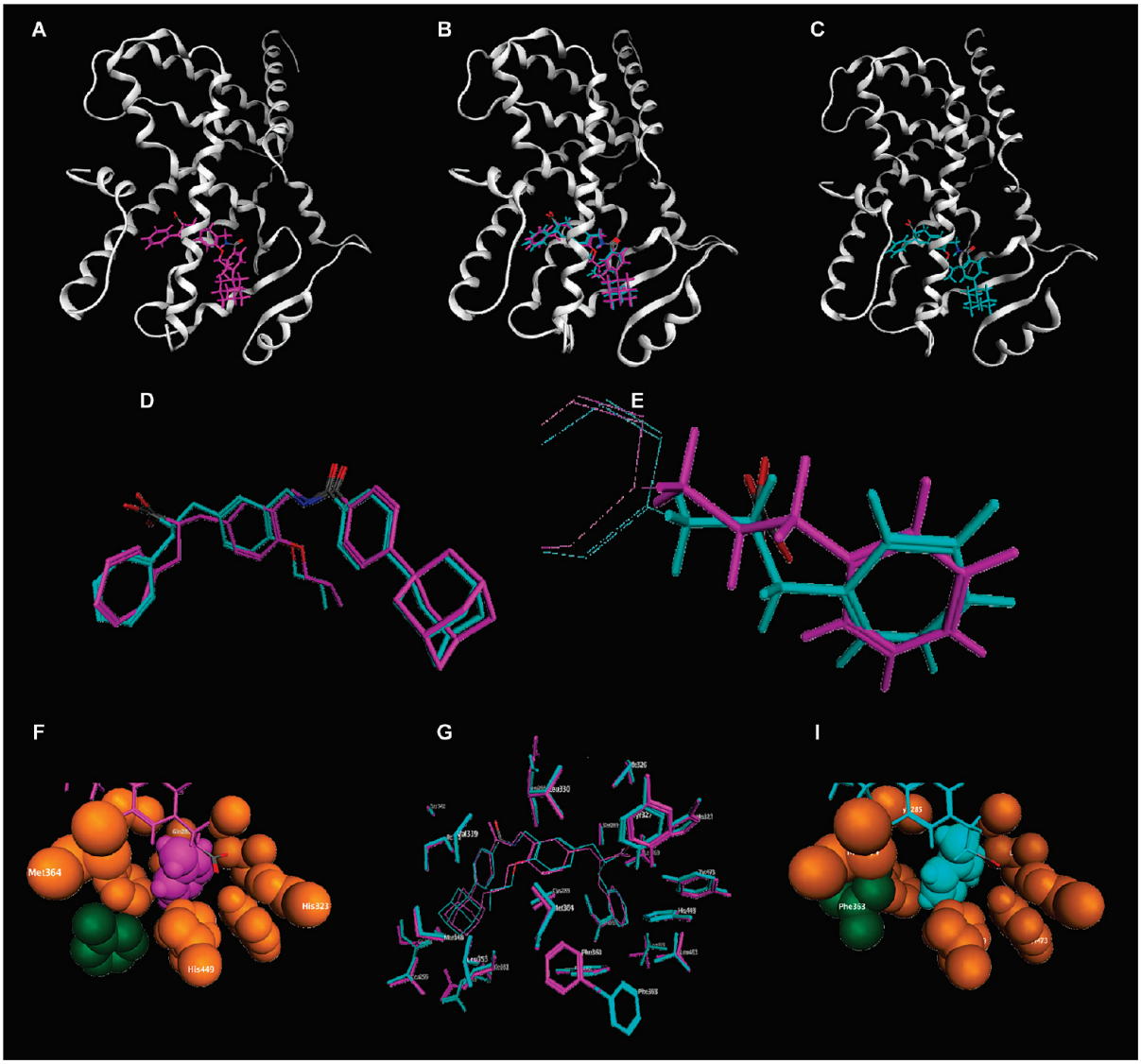

Figure 7. (A,C) Overall crystal structures of hPPARγ LBD−ligand complexes. (A) hPPARγ LBD−(*S*)-**7** complex; (C) hPPARγ LBD−(*R*)-**7** complex. (B) Superposition of the crystal structures of hPPARγ LBD−(*S*)-**7** complex and hPPARγ LBD−(*R*)-**7** complex. Proteins are represented as wireframe models, and (*S*)-**7** and (*R*)-**7** are depicted as cylinder models in magenta ((*S*)-**7**) and cyan ((*R*)-**7** complex). (D) Superposition of the bound structures of (*S*)-**7** and (*R*)-**7**. (E) Zoomed superposition of the conformations of the benzyl group in (*S*)-**7** and (*R*)-**7**. (F,I) Zoomed views of the amino acids of hPPARγ LBD involved in the interaction of the side-chain benzyl group of the ligands. (F) hPPARγ LBD−(*S*)-**7** complex; (I) hPPARγ LBD−(*R*)-**7** complex. The amino acids and the side-chain benzyl groups are depicted as space-filling models in orange (interacting amino acids), magenta (benzyl group of (*S*)-**7**), and cyan (benzyl group of (*R*)-**7**). The flipped Phe363s are highlighted in green. (G) Superposition of the amino acids of hPPARγ LBDs interacting with both (*S*)-**7** and (*R*)-**7**. The main chains are omitted and the side chains are depicted as cylinder models in magenta ((*S*)-**7** complex) and cyan ((*R*)-**7** complex).

A ((*S*)-**7** complex) and C ((*R*)-**7** complex) of Figure 7. Figure 7B presents a superposition of the two complexes. As can be seen from Figure 7D, which is a close-up view of the superposed ligands, the three-dimensional structures of bound (*S*)-**7** and (*R*)-**7** closely resemble each other. The only difference is in the direction of the methylene chain and the configuration of the benzene ring of the α-substituent benzyl group (Figure 7D). It is very surprising that, although the stereochemistry is opposite between (*S*)-**7** and (*R*)-**7**, the benzyl side chains of both ligands are located in the same hydrophobic pocket of hPPARγ LBD formed by the H3, H5, H7, H11, and H12 helixes. This may be the main reason why the (*R*)-enantiomer of **7** exhibited potent hPPARγ transactivation activity, even though the (*R*)-enantiomer is generally thought to be unfavorable, based on the results obtained with compound **6**. It should also be noted that the conformation of the side-chain benzyl group of Phe363 is flipped between hPPARγ LBD complexed with (*S*)-**7** and with (*R*)-**7** (Figure 7F−I). Compared to the (*S*)-**6**-hPPARγ LBD complex, the Phe363 of hPPARγ LBD complexed with (*S*)-**7** exhibits a flipped conformation. Although it is not clear why the conformation of Phe363 is different between the two complex structures, the results of the computational study described below indicated that this conformational change apparently did not contribute to the present stereochemical discrepancy.

2.8. Detailed Analysis of the Interactions of the Side-Chain Benzyl Group of (*R*)-7 and (*S*)-7 Complexed with hPPARγ. We focused on Ser289 and Leu469 in the complex of hPPARγ LBD with (*S*)-**7** and (*R*)-**7** (Figure 8A−D), for Ser289 is the closest amino acid to the methylene chain and the Leu469 is the closest amino acid to the distal benzene ring of the side-chain benzyl group of both (*S*)-**7** and (*R*)-**7**. As described above, the binding modes of the side-chain benzyl group of

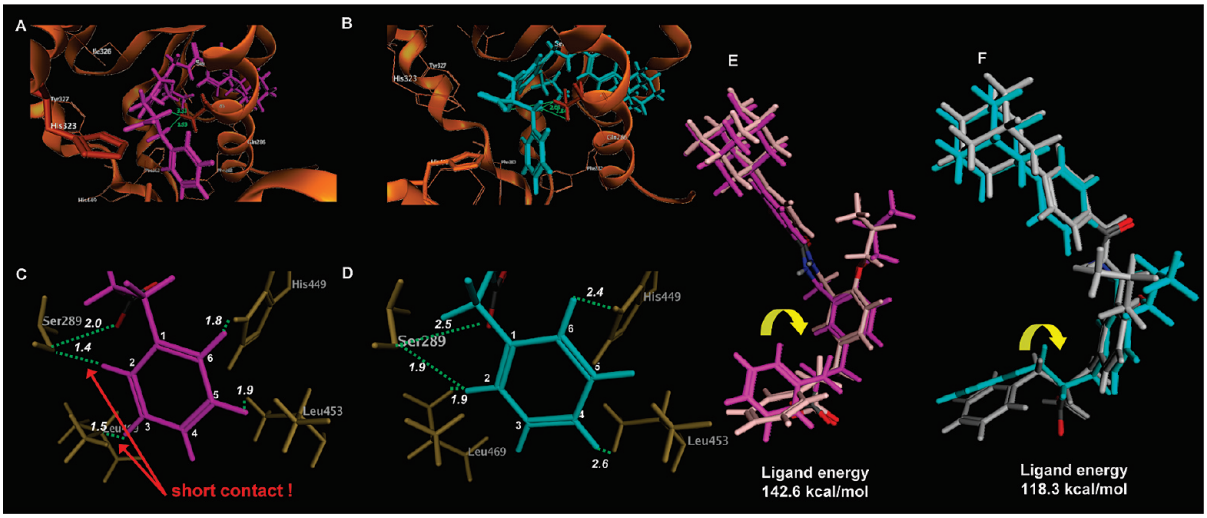

Figure 8. (A) The binding mode of (*S*)-**7** to the ligand-binding pocket of hPPARγ LBD. (B) The binding mode of (*R*)-**7** to the ligand-binding pocket of hPPARγ LBD. Proteins are represented as ribbon models, and the ligands are depicted as cylinder models in magenta ((*S*)-**7**) and cyan ((*R*)-**7**). (C) Zoomed views of the benzyl-binding pocket of hPPARγ LBD−(*S*)-**7** complex. (D) Zoomed views of the benzyl-binding pocket of hPPARγ LBD−(*R*)-**7** complex. The four interacting amino acids are depicted as yellow cylinders, and the benzyl side chains are depicted in magenta ((*S*)-**7**) and cyan ((*R*)-**7** complex). The italic numbers indicate the distance between the indicated atoms (dotted lines). (E) Superposition of the bound structure of (*S*)-**7** and the energy-minimized structure of (*S*)-**7**. (F) Superposition of the bound structure of (*R*)-**7** and the energy-minimized structure of (*R*)-**7**. The calculated ligand energies of the bound ligands are described below. The yellow arrows indicate the directions of distortion of the benzyl groups.

(*S*)-**7** and (*R*)-**7** are similar, but there are significant differences in the detailed protein−ligand interactions. A short contact between the 2-position hydrogen atom of the benzyl group of (*S*)-**7** and the oxygen atom of the side chain of Ser289 was observed, together with a short contact between the 3-position hydrogen atom of the benzyl group of (*S*)-**7** and the hydrogen atom of the side chain of Leu469, with distances of 1.4 and 1.5 Å, respectively. On the other hand, such short contacts were not observed in the case of (*R*)-**7**. This may be one reason why (*S*)-**7** is a weaker hPPARγ agonist than (*R*)-**7**.

The ligand energy calculations of both (*S*)-**7** and (*R*)-**7** also indicated instability of the complex of (*S*)-**7** with hPPARγ LBD. The calculations indicated that the ligand energy of (*S*)-**7** is 142.6 kcal/mol, while that of (*R*)-**7** is 118.3 kcal/mol. Thus, (*S*)-**7** is energetically unstable by 24.3 kcal/mol compared with (*R*)-**7**. As already mentioned, the three-dimensional structures of the bound (*S*)-**7** and (*R*)-**7** are closely similar, and the only differences are the direction of the methylene chain and the configuration of the benzene ring of the α-substituent benzyl group. Therefore, these ligand energy differences might reflect distortion of the side-chain benzyl group of (*S*)-**7** and (*R*)-**7** when bound to hPPARγ LBD. To examine this possibility, we compared the differences of the dihedral angles of the bound benzyl group of these ligands from those of the corresponding energy-minimized structures (Figure 8E,F). The difference of the dihedral angle of the more potent enantiomer, (*R*)-**7**, is about 10°. This indicates that the bound structure of (*R*)-**7** closely resembles the energy-minimized structure. On the contrary, in the case of (*S*)-**7**, a large difference of the dihedral angle, 131°, is observed. This indicated that the benzyl group is substantially distorted when (*S*)-**7** is bound to hPPARγ LBD, and short contacts to Ser289 and Leu469 remain despite the distortion of the benzyl group conformation.

X-ray crystallographic study in combination with computational study indicated that (*S*)-**7** is energetically less stable and somewhat distorted in the complex as compared to (*R*)-**7**. In addition, the conformation and the direction of the side-chain benzyl group of (*S*)-**7** and (*R*)-**7** are different, even though these groups interact with the same binding pocket, and some short contacts can be seen. We suggest that these two factors contribute to the reversal of the stereochemistry-activity relationship in the case of the benzyl derivative.

3. Conclusion

We have designed and synthesized optically active α-benzylphenylpropanoic acid-type hPPARγ-selective agonists in which the key feature is the introduction of a bulky benzyl group at the α-position of the carboxyl group. Interestingly, these compounds showed reversal of the stereochemistry−activity relationship found with other structurally similar α-alkylphenylpropanoic acid PPAR agonists, i.e., (*R*)-**7** is more more potent and hPPARγ-selective than the (*S*)- enantiomer .

The three-point attachment model is generally accepted to explain how receptors and/or enzymes distinguish between enantiomers,[28,29] i.e., three groups arranged around a chiral tetrahedral carbon atom interact with three locations in the active site. Therefore, medicinal chemists sometimes tend to think that a consistent tendency will be observed in a series of compounds with the same basic framework. However, the present results show that this is not necessarily the case. So, double-checking by making several analogues in both enantiomeric series is important.

Our analysis also demonstrates that X-ray crystallographic analysis combined with computational chemistry is a powerful tool to investigate three-dimensional structure−activity relationships in detail.

4. Experimental Section

4.1. Chemistry. 4.1.1. General Methods. Melting points were determined with a Yanagimoto hot-stage melting point apparatus and are uncorrected. NMR spectra were recorded on a VarianVXR-300 (1H 300 MHz) spectrometer. Proton chemical

shifts were referenced to the TMS internal standard. Elemental analysis was carried out with a Yanagimoto MT-5 CHN recorder elemental analyzer and results were within 0.4% of the theoretical values. FAB-MS was carried out with a VG70-SE. Chemical purity was determined by HPLC analysis with a Pegasil ODS SP100 column (4.6 mm ×150 mm; flow rate of 1 mL/min; solvent, MeCN:0.1% TFA = 3:1 v/v; detection at 254 nm), confirming >98% purity.

4.1.2. Benzyl 2-Propoxy-5-formylbenzoate (9). A mixture of 5-formylsalicylic acid (**8**) (2.50 g, 15.0 mmol), benzyl bromide (1.79 mL, 15.1 mmol), potassium hydrogencarbonate (1.51 g, 15.1 mmol), and 40 mL of *N*,*N*-dimethylformamide was stirred at room temperature for 24 h. The mixture was poured into ice−water, and stirring was continued for 1 h. The precipitate was collected by filtration and redissolved in 100 mL of AcOEt. This solution was dried over anhyd $MgSO_4$, filtered, and concentrated to obtain 3.54 g of benzyl 5-formylsalicylate. A mixture of this product (2.00 g, 7.80 mmol), iodopropane (1.14 mL, 11.7 mmol), potassium carbonate (1.62 g, 11.7 mmol), and 30 mL of *N*,*N*-dimethylformamide was stirred at 60 °C for 24 h. The reaction mixture was poured into water, and the whole was extracted with ethyl acetate. The organic solution was washed with water and brine, dried over anhydrous magnesium sulfate, and concentrated. The residue was purified by silica gel column chromatography (eluant; *n*-hexane:ethyl acetate = 3:1 v/v) to afford 2.53 g (quant.) of the title compound as a colorless powder. ^{1}H NMR (400 MHz, $CDCl_3$) δ 9.90 (s, 1H), 8.33 (d, J= 2.0 Hz, 1H), 7.99 (dd, J = 8.6, 2.2 Hz, 1H), 7.46 (dd, J = 8.0, 1.2 Hz, 2H), 7.41−7.31 (m, 3H), 7.07 (d, J = 8.8 Hz, 1H), 5.37 (s, 2H), 4.08 (t, J = 6.4 Hz, 2H), 1.89−1.80 (m, 2H), 1.01 (t, J = 7.4 Hz, 3H). MS (FAB) m/z 299 ($M + H^+$).

4.1.3. Benzyl 5-Hydroxymethyl-2-propoxybenzoate (10). To a solution of **9** (2.53 g, 8.48 mmol), and 30 mL of ethanol was added $NaBH_4$ (160 mg, 4.23 mmol) portionwise at 0 °C, and the mixture was stirred for 2 h at room temperature. The excess ethanol was evaporated, the residue was poured into water, and the whole was extracted with ethyl acetate. The extract was washed with water and brine, dried over anhydrous magnesium sulfate, and concentrated. The residue was purified by silica gel column chromatography (eluant; *n*-hexane:ethyl acetate = 3:1 v/v) to afford 2.33 g (91%) of the title compound as a colorless oil. ^{1}H NMR (400 MHz, $CDCl_3$) δ 7.79 (d, J = 2.4 Hz, 1H), 7.46−7.44 (m, 3H), 7.39−7.31 (m, 3H), 6.94 (d, J=8.4 Hz, 1H), 5.37 (s, 2H), 4.62 (s, 2H), 3.98 (t, J = 6.4 Hz, 2H), 1.85−1.76 (m, 2H), 0.99 (t, J = 7.4 Hz, 3H). MS (FAB) m/z 301 ($M + H^+$).

4.1.4. Benzyl 5-Bromomethyl-2-propoxybenzoate (11). A mixture of **10** (2.33 g, 7.76 mmol), phosphorus tribromide (0.74 mL, 7.79 mmol), and 30 mL of dehydrated ether was stirred for 1.5 h at 0 °C. The reaction mixture was poured into water, and the whole was extracted with ether. The extract was washed with water and brine, dried over anhydrous magnesium sulfate, and concentrated. The residue was purified by silica gel column chromatography (eluant; *n*-hexane:ethyl acetate = 3:1 v/v) to afford 1.43 g (52%) of the title compound as a colorless oil. ^{1}H NMR (400 MHz, $CDCl_3$) δ 7.84 (d, J = 2.4 Hz, 1H), 7.49−7.44 (m, 3H), 7.40−7.31 (m, 3H), 6.92 (d, J=8.4 Hz, 1H), 5.35 (s, 2H), 4.47 (s, 2H), 3.98 (t, J = 6.4 Hz, 2H), 1.84−1.76 (m, 2H), 0.98 (t, J = 7.4 Hz, 3H).

4.1.5. Benzyl 5-((*R*)-2-Benzyl-3-((*S*)-4-benzyl-2-oxo-oxazolidin-3-yl)-3-oxopropyl)-2-propoxy-benzoate (12). (*R*)-3-(3-Phenylpropanoyl)-4-benzyloxazolidin-2-one (0.74 g, 2.33 mmol) and 20 mL of dehydrated tetrahydrofuran were mixed under an argon atmosphere and cooled to −50 °C. Under stirring, a 1 mol/L solution of sodium bis(trimethylsilyl)amide in dehydrated tetrahydrofuran (8.00 mL, 8.00 mmol) was added dropwise. After completion of the addition, the mixture was stirred for 1 h at −15 °C and recooled to −50 °C, and then a solution of **11** (0.86 g, 2.37 mmol) in dehydrated tetrahydrofuran (20 mL) was added dropwise. After completion of the addition, the mixture was further stirred for 1 h while being gradually heated to room temperature. A saturated aqueous solution of ammonium chloride was added to the reaction mixture, and the whole was extracted with ethyl acetate. The extract was washed with water and brine, dried over anhydrous sodium sulfate, and concentrated. The residue was purified by silica gel chromatography (eluant; *n*-hexane:ethyl acetate = 9: 2 v/v) to afford 0.87 g (64%) of the desired compound as a colorless oil. ^{1}H NMR (400 MHz, $CDCl_3$) δ 7.70 (d, J = 2.4 Hz, 1H), 7.44−7.16 (m, 14H), 6.98 (dd, J = 7.6, 1.6 Hz, 2H), 6.87 (d, J = 8.4 Hz, 1H), 5.29 (s, 2H), 4.60−4.52 (m, 1H), 4.42−4.36 (m, 1H), 3.97−3.88 (m, 3H), 3.78 (t, J = 8.4 Hz, 1H), 3.09 (dd, J = 13.6, 8.8 Hz, 1H), 3.03−2.96 (m, 2H), 2.85−2.76 (m, 2H), 2.44 (dd, J = 13.6, 9.6 Hz, 1H), 1.81−1.72 (m, 2H), 0.96 (t, J = 7.4 Hz, 3H). MS (FAB) m/z 592 ($M + H^+$).

4.1.6. 5-((*R*)-2-Benzyl-3-((*S*)-4-benzyl-2-oxo-oxazolidin-3-yl)-3-oxopropyl)-2-propoxybenzoic Acid (13). Compound **12** (0.89 g, 1.50 mmol), 200 mg of 10% palladium on carbon, and 80 mL of ethyl acetate were mixed and catalytic hydrogenation was carried out at an initial hydrogen pressure of 98 kPa. After completion of the reaction, the catalyst was removed by filtration and the filtrate was washed with ethyl acetate. The reaction mixture and the washings were combined and concentrated. The residue was purified by silica gel chromatography (eluant; *n*-hexane:ethyl acetate = 5:2 v/v) to afford 0.41 g (55%) of the desired compound as a colorless oil. ^{1}H NMR (400 MHz, $CDCl_3$) δ 10.98 (s, 1H), 8.06 (d, J = 2.4 Hz, 1H), 7.52 (dd, J = 8.4, 2.4 Hz, 1H), 7.24−7.22 (m, 5H), 7.20−7.16 (m, 3H), 7.03 (dd, J = 7.2, 2.0 Hz, 2H), 6.97 (d, J = 8.4 Hz, 1H), 4.56−4.48 (m, 1H), 4.46−4.40 (m, 1H), 4.22−4.13 (m, 2H), 3.97 (dd, J = 8.8, 2.4 Hz, 1H), 3.81 (t, J = 8.2 Hz, 1H), 3.16 (dd, J = 13.8. 8.2 Hz, 1H), 3.08−2.98 (m, 2H), 2.84−2.76 (m, 2H), 2.54 (dd, J = 13.4, 9.4 Hz, 1H), 1.96−1.88 (m, 2H), 1.08 (t, J = 7.2 Hz, 3H). MS (FAB) m/z 502 ($M + H^+$).

4.1.7. 5-((*S*)-2-((*R*)-4-Benzyl-2-oxo-oxazolidine-3-carbonyl)-butyl)2-*n*-butoxybenzylaldehyde (14). To a solution of **13** (1.37 g, 3.02 mmol) and 25 mL of dehydrated tetrahydrofuran was added dropwise a 1 mol/L solution of borane−tetrahydrofuran complex (5.00 mL, 5.00 mmol). After completion of the addition, the mixture was stirred overnight at room temperature. A saturated aqueous solution of ammonium chloride was added to the reaction mixture, and the whole was extracted with ethyl acetate. The extract was washed with water and brine, dried over anhydrous sodium sulfate, and concentrated. The residue was purified by silica gel chromatography (eluant; *n*-hexane:ethyl acetate = 4:1 v/v) to afford 1.18 g (89%) of the intermediate hydroxymethyl derivative as a colorless oil. A solution of the hydroxymethyl derivative (1.18 g, 2.68 mmol), activated MnO_2 (0.50 g, 5.75 mmol), and 30 mL of dehydrated dichloromethane was stirred overnight at room temperature. The catalyst was collected by filtration, washed with dichloromethane, and concentrated. The residue was purified by silica gel chromatography (eluant; *n*-hexane:ethyl acetate=4:1 v/v) to afford 855 mg (73%) of the desired compound as a colorless oil. ^{1}H NMR (500 MHz, $CDCl_3$) δ 8.05 (d, J=2.3 Hz, 1H), 7.52 (dd, J=8.5, 2.3 Hz, 1H), 7.29−7.24 (m, 3H), 7.08 (d, J=6.8 Hz, 2H), 6.97 (d, J=8.5 Hz, 1H), 4.68 (m, 1H), 4.24−4.01 (m, 5H), 3.14 (dd, J=13.2, 3.4 Hz, 1H), 3.08 (dd, J=13.7, 7.7 Hz, 1H), 2.77 (dd, J=13.7, 6.8 Hz, 1H), 2.58 (dd, J=13.2, 9.8 Hz, 1H), 1.87 (m, 2H), 1.77 (m, 1H), 1.51 (m, 3H), 0.99 (t, J=7.3 Hz, 3H), 0.93 (t, J=7.3 Hz, 3H). MS (FAB) 454 $(M + H)^+$.

4.1.8. *N*-((5-((*R*)-2-Benzyl-3-((*S*)-4-benzyl-2-oxo-oxazolidin-3-yl)-3-oxopropyl)-2-propoxy-phenyl)methyl)-4-(1-adamantyl)-benzamide (15). A mixture of **14** (200 mg, 0.41 mmol), 4-(1-adamantyl)benzamide (270 mg, 1.03 mmol), triethylsilane (0.16 mL, 1.03 mmol), trifluoroacetic acid (0.08 mL, 1.03 mmol), and 30 mL of dehydrated toluene was refluxed for 2 days. The mixture was evaporated, and the residue was purified by silica gel column chromatography (eluant; *n*-hexane:ethyl acetate=2:1 v/v) to afford 290 mg (97%) of the title compound as a colorless oil. ^{1}H NMR (300 MHz, $CDCl_3$) δ 7.61 (d, J = 8.7 Hz, 2H), 7.35 (d, J = 8.7 Hz, 2H), 7.28−7.16 (m, 10H), 6.88−6.85 (m, 2H), 6.80

(d, J = 8.4 Hz, 1H), 6.71 (t, J = 5.7 Hz, 1H), 4.70−4.52 (m, 3H), 4.42−4.34 (m, 1H), 3.98−3.88 (m, 3H), 3.74 (t, J = 8.4 Hz, 1H), 3.07 (dd, J = 13.8, 8.7 Hz, 1H), 3.01−2.84 (m, 2H), 2.79 (dd, J = 13.8, 6.3 Hz, 2H), 2.48 (dd, J = 13.2, 9.0 Hz, 1H), 2.10 (s, 3H), 1.89−1.72 (m, 14H), 1.03 (t, J = 7.5 Hz, 3H). MS (FAB) m/z 725 ($M + H^+$).

4.1.9. (*R*)-2-Benzyl-3-(3-(((4-adamantan-1-yl)benzamido)methyl)-4-propoxyphenyl)propanoic Acid ((*R*)-7). Compound **15** (290 mg, 0.400 mol) was dissolved in 24 mL of tetrahydrofuran and 6 mL of water under an argon atmosphere with ice-cooling. To this solution was added 30% aqueous hydrogen peroxide (0.4 mL, 4.00 mmol). Then a solution of lithium hydroxide monohydrate (100 mg, 2.38 mmol) in water (1 mL) was added, and the mixture was stirred further for 2.5 h at 0 °C, and for 3 h at room temperature. An aqueous solution of sodium hydrogen sulfite (1.00 g/6 mL) was added to the mixture, and the whole was stirred for 30 min. The reaction mixture was acidified with diluted HCl and then extracted with ethyl acetate. The extract was washed with brine, dried over anhydrous magnesium sulfate, and concentrated. The residue was purified by silica gel column chromatography (eluant; *n*-hexane:ethyl acetate = 2:1 v/v) to afford 190 mg (86%) of the title compound as a colorless powder; mp 177−178 °C. ^{1}H NMR (300 MHz, $CDCl_3$) δ 7.68 (d, J = 8.1 Hz, 2H), 7.39 (d, J = 8.4 Hz, 2H), 7.26−7.14 (m, 6H), 7.03 (dd, J = 8.1, 1.8 Hz, 1H), 6.77−6.70 (m, 2H), 4.64−4.51 (m, 2H), 3.94 (t, J = 6.5 Hz, 2H), 3.01−2.71 (m, 5H), 2.10 (s, 3H), 1.90−1.72 (m, 14H), 1.06 (t, J = 7.4 Hz, 3H). HRMS (FAB, MH^+) calcd for $C_{36}H_{24}Cl_3N_2O_5$ 566.3270, found 566.3282. $[\alpha]_D$ −3° (c 0.10, CH_3CN). Anal. ($C_{37}H_{44}NO_4$) C, H, N.

4.1.10. (*S*)-2-Benzyl-3-(3-(((4-adamantan-1-yl)benzamido)-methyl)-4-propoxyphenyl)propanoic Acid ((*S*)-7). This compound was prepared by means of a procedure similar to that used for (*R*)-**7**; mp 177−178 °C. ^{1}H NMR (300 MHz, $CDCl_3$) δ 7.68 (d, J = 8.1 Hz, 2H), 7.39 (d, J = 8.1 Hz, 2H), 7.26−7.14 (m, 6H), 7.03 (dd, J = 8.1, 1.8 Hz, 1H), 6.77−6.70 (m, 2H), 4.64−4.51 (m, 2H), 3.94 (t, J = 6.5 Hz, 2H), 3.01−2.71 (m, 5H), 2.10 (s, 3H), 1.90−1.72 (m, 14H), 1.06 (t, J = 7.4 Hz, 3H). HRMS (FAB, MH^+) calcd for $C_{36}H_{24}Cl_3N_2O_5$ 566.3270, found 566.3265. $[\alpha]_D$ +3° (c 0.10, CH_3CN). Anal. ($C_{37}H_{44}NO_4 \cdot {}^1/_4H_2O$) C, H, N.

4.2. Cell Culture and Transactivation Assays. Human embryonic kidney HEK293 cells were cultured in Dulbecco's Modified Eagle's Medium (DMEM) containing 5% fetal bovine serum and antibiotic−antimycotic mixture (Nacalai) at 37 °C in a humidified atmosphere of 5% CO_2 in air. Transfections were performed by means of the calcium phosphate coprecipitation method. Eight hours after transfection, test compounds were added. Cells were harvested approximately 16−20 h after the treatment, and luciferase and β-galactosidase activities were measured with a luminometer and a microplate reader. DNA cotransfection experiments included 50 ng of reporter plasmid, 20 ng of pCMX-ss-galactosidase, 15 ng of each receptor expression plasmid, and pGEM carrier DNA to make a total of 150 ng of DNA per well in a 96-well plate. Luciferase data were normalized to an internal β-galactosidase control and reported values are the means of triplicate assays.

4.3. X-ray Crystallography of the Ligand/PPAR-LBD Complex. Determination of the **4**-hPPARα LBD, the **5**-hPPARδ LBD, and the **6**-hPPARγ LBD cocrystal structures, including protein purification, crystal growth, and structural refinement, was performed as described previously.[23]

The human PPARγ LBD (aa 203−477) was purified as described previously.[30] All crystals were prepared through cocrystallization with (*R*)-**7** or (*S*)-**7** under the same conditions to permit straightforward comparison between the two structures. An aliquot (2 μL) of protein solution (15 mg/mL in 20 mmol/L Tris, pH 8.0, 150 mmol/L NaCl) was mixed with an equal volume of 0.1 mmol/L ligand solution (0.8 mol/L sodium citrate, 100 mmol/L HEPES, pH 7.5, 1% DMSO), and then crystallization of the ligand/protein mixture was achieved by the hanging drop vapor diffusion method at 293K. Crystals were flash-cooled in a liquid nitrogen stream after they had been briefly soaked in cryoprotection buffer (1.1 mol/L sodium citrate, 100 mmol/L HEPES, pH 7.5, and 25% (v/v) glycerol). Diffraction data were collected at BL38B1 in SPring-8 (Harima, Japan). All data were processed using HKL2000.[31] All structures were solved by the molecular replacement method, using the previously published structure of the **6**-hPPARγ LBD complex (PDB 2ZNO)[23] as a probe after removing the ligand part. The correctly positioned molecules were refined with CNS[32] and O.[33] The crystallographic data and refinement statistics are summarized in Table 1. The coordinates of hPPARγ LBD−(*S*)-**7** and hPPARγ LBD−(*R*)-**7** complexes have been deposited in the Brookhaven Protein Data Bank (PDB) with the codes of 3AN3 and 3AN4, respectively.

4.4. Computational Study to Calculate Strain Energies of the (*R*)-7 and (*S*)-7. Each binding conformation of (*R*)-**7** and (*S*)-**7** was extracted from each X-ray complex structure. The strain energies of the binding conformations of (*R*)-**7** and (*S*)-**7** were calculated using the Tripos force field in SYBYL7.3.

Acknowledgment. This work was supported in part by the Targeted Proteins Research Program of the Japan Science and Technology Corporation (JST) and by the Uehara Memorial Foundation, and the Teromo Life Science Foundation. We are grateful to Drs. Seiki Baba and Nobuhiro Mizuno for their kind help in the X-ray diffraction data collection on BL38B1 at SPring-8. We thank Dr. Tsuyoshi Waku and Rinna Nakamori for their help in crystallization. T.O. and K.M. were supported by a Grant-in-Aid for Creative Scientific Research Program (18GS0316) from the Japan Society for the Promotion of Science (JSPS).

Supporting Information Available: Combustion analysis data for (*R*)-**7** and (*S*)-**7**. This material is available free of charge via the Internet at http://pubs.acs.org.

References

(1) Chawla, A.; Repa, J. J.; Evans, R. M.; Mangelsdorf, D. J. Nuclear receptors and lipid physiology: opening the X-files. *Science* **2001**, *294*, 1866–1870.
(2) Banner, C. D.; Göttlicher, M.; Widmark, E.; Sjövall, J.; Rafter, J. J.; Gustafsson, J. A. Systematic analytical chemistry/cell assay approach to isolate activators of orphan nuclear receptors from biological extracts: characterization of peroxisome proliferator-activated receptor activators in plasma. *J. Lipid Res.* **1993**, *34*, 1583–1591.
(3) Braissant, O.; Foufelle, F.; Scotto, C.; Dauca, M.; Wahli, W. Differential expression of peroxisome proliferator-activated receptors (PPARs): tissue distribution of PPAR-alpha, -beta, and -gamma in the adult rat. *Endocrinology*. **1996**, *137*, 354–366.
(4) Spiegelman, B. M.; Hu, E.; Kim, J. B.; Brun, R. PPAR gamma and the control of adipogenesis. *Biochimie* **1997**, *79*, 111–112.
(5) Okuno, A.; Tamemoto, H.; Tobe, K.; Ueki, K.; Mori, Y.; Iwamoto, K.; Umesono, K.; Akanuma, Y.; Fujiwara, T.; Horikoshi, H.; Yazaki, Y.; Kadowaki, T. Troglitazone increases the number of small adipocytes without the change of white adipose tissue mass in obese Zucker rats. *J. Clin. Invest.* **1998**, *101*, 1354–1361.
(6) Mendez, M.; LaPointe, M. C. PPARgamma inhibition of cyclooxygenase-2, PGE2 synthase, and inducible nitric oxide synthase in cardiac myocytes. *Hypertension* **2003**, *42*, 844–850.
(7) Morrison, R. F.; Farmer, S. R. Role of PPARgamma in regulating a cascade expression of cyclin-dependent kinase inhibitors, p18(INK4c) and p21(Waf1/Cip1), during adipogenesis. *J. Biol. Chem.* **1999**, *274*, 17088–17097.
(8) Huang, J. W.; Shiau, C. W.; Yang, J.; Wang, D. S.; Chiu, H. C.; Chen, C. Y.; Chen, C. S. Development of small-molecule cyclin D1-ablative agents. *J. Med. Chem.* **2006**, *49*, 4684–4689.
(9) Chaplain, M. A.; McDougall, S. R.; Anderson, A. R. Mathematical modeling of tumor-induced angiogenesis. *Annu. Rev. Biomed. Eng.* **2006**, *8*, 233–257.
(10) Sato, M. Peroxisome proliferator activated receptor ligands and angiogenesis. *Nippon Rinsho* **2005**, *63*, 603–608.
(11) Lehmann, J. M.; Moore, L. B.; Smith-Oliver, T. A.; Wilkison, W. O.; Willson, T. M.; Kliewer, S. A. An antidiabetic thiazolidinedione is a

high affinity ligand for peroxisome proliferator-activated receptor gamma (PPAR gamma). *J. Biol. Chem.* **1995**, *270*, 12953–12956.
(12) Hashimoto, Y.; Miyachi, H. Nuclear receptor antagonists designed based on the helix-folding inhibition hypothesis. *Bioorg. Med. Chem.* **2005**, *13*, 5080–5093.
(13) Nomura, M.; Tanase, T.; Ide, T.; Tsunoda, M.; Suzuki, M.; Uchiki, H.; Murakami, K.; Miyachi, H. Design, synthesis and evaluation of substituted phenylpropanoic acid derivatives as human peroxisome proliferator-activated receptor activators; discovery of potent and human PPARα subtype-selective activators. *J. Med. Chem.* **2003**, *46*, 3581–3599.
(14) Kasuga, J.; Yamasaki, D.; Araya, Y.; Nakagawa, A.; Makishima, M.; Doi, T.; Hashimoto, Y.; Miyachi, H. Design, synthesis and evaluation of a novel series of α-substituted phenylpropanoic acid derivatives as human peroxisome proliferator-activated receptor (PPAR) alpha/delta dual agonists for the treatment of metabolic syndrome. *Bioorg. Med. Chem.* **2006**, *14*, 8405–8414.
(15) Kasuga, J.; Nakagome, I.; Aoyama, A.; Sako, K.; Ishizawa, M.; Ogura, M.; Makishima, M.; Hirono, S.; Hashimoto, Y.; Miyachi, H. Design, synthesis, and evaluation of potent, structurally novel peroxisome proliferator-activated receptor (PPAR) delta-selective agonists. *Bioorg. Med. Chem.* **2007**, *15*, 5177–5190.
(16) Kasuga, J.; Yamasaki, D.; Ogura, K.; Shimizu, M.; Sato, M.; Makishima, M.; Doi, T.; Hashimoto, Y.; Miyachi, H. SAR-oriented discovery of peroxisome proliferator-activated receptor pan agonist with a 4-adamantylphenyl group as a hydrophobic tail. *Bioorg. Med. Chem. Lett.* **2008**, *18*, 1110–1105.
(17) Xu, H. E.; Lambert, M. H.; Montana, V. G.; Plunket, K. D.; Moore, L. B.; Collins, J. L.; Oplinger, J. A.; Kliewer, S. A.; Gampe, R. T., Jr.; McKee, D. D.; Moore, J. T.; Willson, T. M. Structural determinants of ligand binding selectivity between the peroxisome proliferator-activated receptors. *Proc. Natl. Acad. Sci. U.S.A.* **2001**, *98*, 13919–13924.
(18) Evans, D. A.; Ennis, M. D.; Mathre, D. J. Asymmetric alkylation reactions of chiral imide enolates. A practical approach to the enantioselective synthesis of alpha-substituted carboxylic acid derivatives. *J. Am. Chem. Soc.* **1982**, *104*, 1737–1739.
(19) The enantiomeric excess was determined with a CHIRALPAK AD-H column, with hexane/*i*-PrOH/trifluoroacetic acid = 90:10: 0.1 v/v/v as the mobile phase, at a flow rate of 0.5 mL/min, with detection at 254 nm.
(20) Sznaidman, M. L.; Haffner, C. D.; Maloney, P. R.; Fivush, A.; Chao, E.; Goreham, D.; Sierra, M. L.; LeGrumelec, C.; Xu, H. E.; Montana, V. G.; Lambert, M. H.; Willson, T. M.; Oliver, W. R., Jr.; Sternbach, D. D. Novel selective small molecule agonists for peroxisome proliferator-activated receptor delta (PPARdelta); synthesis and biological activity. *Bioorg. Med. Chem. Lett.* **2003**, *13*, 1517–1521.
(21) Cobb, J. E.; Blanchard, S. G.; Boswell, E. G.; Brown, K. K.; Charifson, P. S.; Cooper, J. P.; Collins, J. L.; Dezube, M.; Henke, B. R.; Hull-Ryde, E. A.; Lake, D. H.; Lenhard, J. M.; Oliver, W., Jr.; Oplinger, J.; Pentti, M.; Parks, D. J.; Plunket, K. D.; Tong, W. Q. *N*-(2-Benzoylphenyl)-L-tyrosine PPARgamma agonists. 3. Structure−activity relationship and optimization of the *N*-aryl substituent. *J. Med. Chem.* **1998**, *41*, 5055–5069.
(22) Hulin, B.; Newton, L. S.; Lewis, D. M.; Genereux, P. E.; Gibbs, E. M.; Clark, D. A. Hypoglycemic activity of a series of alpha-alkylthio and alpha-alkoxy carboxylic acids related to ciglitazone. *J. Med. Chem.* **1996**, *39*, 3897–3907.
(23) Oyama, T.; Toyota, K.; Waku, T; Hirakawa, Y.; Nagasawa, N.; Kasuga, J.; Hashimoto, Y.; Miyachi, H.; Morikawa, K. Adaptability and selectivity of human peroxisome proliferator-activated receptor (PPAR) pan agonists revealed from crystal structures. *Acta Crystallogr., Sect. D: Biol. Crystallogr.* **2009**, *65*, 786–795.
(24) Computer-graphic work was performed using MOE (Molecular Operating Environment) (Ryoka Systems Inc.).
(25) Nolte, R. T.; Wisely, G. B.; Westin, S.; Cobb, J. E.; Lambert, M. H; Kurokawa, R.; Rosenfeld, M. G.; Willson, T. M.; Glass, C. K.; Milburn, M. V. Ligand binding and co-activator assembly of the peroxisome proliferator-activated receptor-gamma. *Nature* **1998**, *395*, 137–143.
(26) Rosenfeld, M. G.; Lunyak, V. V.; Glass, C. K. Sensors and signals: a coactivator/corepressor/epigenetic code for integrating signal-dependent programs of transcriptional response. *Genes Dev.* **2006**, *20*, 1405–1428.
(27) Nagy, L.; Kao, H. Y.; Love, J. D.; Li, C.; Banayo, E.; Gooch, J. T.; Krishna, V.; Chatterjee, K.; Evans, R. M.; Schwabe, J. W. Mechanism of corepressor binding and release from nuclear hormone receptors. *Genes Dev.* **1999**, *13*, 3209–3216.
(28) Ogston, A. G. Interpretation of experiments on metabolic processes, using isotopic tracer elements. *Nature* **1948**, *163*, 963.
(29) Easson, L. H.; Stedman, E. Studies on the relationship between chemical constitution and physiological action—Molecular dissymmetry and physiological activity. *Biochem. J.* **1933**, *27*, 1257–1266.
(30) Waku, T.; Shiraki, T.; Oyama, T.; Fujimoto, Y.; Maebara, K.; Kamiya, N.; Jingami, H.; Morikawa, K. Structural insight into PPARgamma activation through covalent modification with endogenous fatty acids. *J. Mol. Biol.* **2009**, *385*, 188–199.
(31) Otwinowski, Z.; Minor, W. *Methods Enzymol.* **1997**, *276*, 307–326.
(32) Brünger, A. T.; Adams, P. D.; Clore, G. M.; DeLano, W. L.; Gros, P.; Grosse-Kunstleve, R. W.; Jiang, J.-S.; Kuszewski, J.; Nilges, M.; Pannu, N. S.; Read, R. J.; Rice, L. M.; Simonson, T.; Warren, G. L. Crystallography & NMR system: A new software suite for macromolecular structure determination. *Acta Crystallogr.* **1998**, *D54*, 905–921.
(33) Jones, T. A.; Zou, J.-Y.; Cowan, S. W.; Kjeldgaard, M. Improved methods for building protein models in electron density maps and the location of errors in these models. *Acta Crystallogr.* **1991**, *A47*, 110–119.